XVII Congresso Brasileiro de Mecânica dos Solos e Engenharia Geotécnica
VII Congresso Luso-Brasileiro de Geotecnia
VI Simpósio Brasileiro de Mecânica das Rochas
VI Simpósio Brasileiro de Jovens Geotécnicos
COBRAMSEG 2014
9 a 13 de setembro de 2014 - Goiânia/GO - Brasil

Soil stabilization with alkaline activated fly ash

Sara Rios
Departamento de Engenharia Civil, Universidade do Porto, Porto, Portugal, sara.rios@fe.up.pt

António Viana da Fonseca
Departamento de Engenharia Civil, Universidade do Porto, Porto, Portugal, viana@fe.up.pt

SUMMARY: Mixtures of silty sand, fly ash and an alkaline solution were tested in unconfined compression at 90 days of curing for evaluation of strength and, stiffness using local strain instrumentation. Measurements of seismic wave velocities were performed during the curing period, in order to evaluate the material geomechanical behavior evolution with time. These results were also compared with a specimen of soil and fly ash without alkali activator to analyze the effect of the activator. A significant increase in strength and stiffness due to the activator was observed which highlights the potential of this technique as a cement replacement bonding agent. The use of waste products like fly ash instead of cement makes this technique especially respectable for the environment, prospectively competitive economically and friendly for the sustainability of our resources.

KEYWORDS: Soil improvement, alkaline activation, seismic wave velocities, fly ash.

1 INTRODUCTION

Soil stabilization is generally performed by the addition of Portland cement which has a negative environmental impact since its production releases a considerable amount of carbon dioxide (CO_2) to the atmosphere. It is estimated that the cement industry contributes about 5% to global anthropogenic CO_2 emissions, making the cement industry an important sector for CO_2-emission mitigation strategies (Worrell et al., 2001).

The use of waste materials in the construction industry is an important contribution for the reduction in cement consumption. Particularly, the use of fly ash has become more prevalent. It is produced from the burning of coal, and consists of the inorganic matter that did not burn during the process. The amorphous chemical structure of fly ash, which is a consequence of the high temperatures it has been subjected to during combustion, makes it particularly interesting for alkaline activation.

In general terms, alkaline activation is a reaction between alumina-silicate materials and alkali or alkali earth substances, namely alkaline ions like sodium or potassium, or alkaline earth ions like calcium. It can be described as a polycondensation process, in which the silica and alumina units interconnect and share the oxygen ions. Materials formed using reactions between silica and alumina and alkali cations like sodium or potassium are very similar, at a molecular level, with natural rocks, sharing their stiffness, durability and strength.

The alkaline activation of fly ash to create a new binder alternative to Portland cement has been successfully applied to replace the traditional Portland cement concrete (Alonso and Palomo, 2001). However, few applications have been carried out in soil improvement, and in all the known cases the treatment was carried out by low pressure grouting or superficial soil mixing (Cristelo et al., 2011, 2013), techniques that are not always feasible.

In this paper mixtures of soil, fly ash and an alkaline solution were mixed together to evaluate the evolution of strength and stiffness with time.

2 MATERIALS AND METHODS

2.1 Soil, fly ash and alkaline solution

The soil involved in this research program is classified as silty sand according to the Unified Classification System (ASTM, 1998). It results from the weathering of Porto granite, a rather abundant rock in the north and central regions of Portugal. The particle size distribution plotted in Figure 1 shows evidence of a very well graded soil containing about 30% fines. The specific gravity of the solids was determined as 2.72. The effective diameter, D_{50}, is 0.25 mm, with uniformity and curvature coefficients of 113 and 2.7 respectively (Viana da Fonseca et al., 2013).

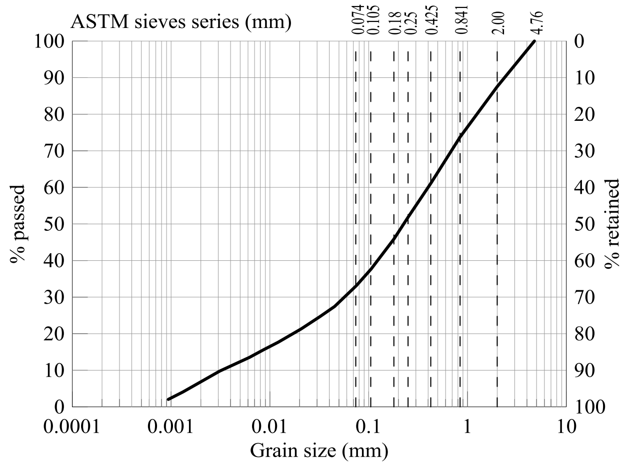

Figure 1. Grain size distribution of the soil known as Porto silty sand

Type F fly ash was used in the alkaline activation obtained from a coal thermoelectric power plant in central Portugal.

The alkaline solution comprised sodium hydroxide and sodium silicate. Sodium hydroxide in flake form with a specific gravity of 2.13 at 20ºC and 95-99% purity was dissolved in water up to the desired concentration. The sodium silicate was already in solution form with a specific gravity of 1.5 and S_iO_2/Na_2O ratio of 2 by mass.

2.2 Specimen preparation

Soil and fly ash were dry mixed until complete homogenization using a mason spoon, joining afterwards the alkaline activator with additional mixing. The mixture was statically compacted in three layers in a lubricated mold of 70 mm of diameter and 140 mm of height. The specimens extracted from the mold were left to cure in a room with controlled temperature (20º C) and humidity (95%) inside plastic bags to avoid moisture loss.

The compaction condition of the specimens was defined from the Modified Proctor curve (Figure 2) at the optimum point obtained for the mixture of soil and fly ash. A fly ash content of 10% was selected for all the mixtures, defined as the mass of fly ash divided by the mass of solids (soil and fly ash).

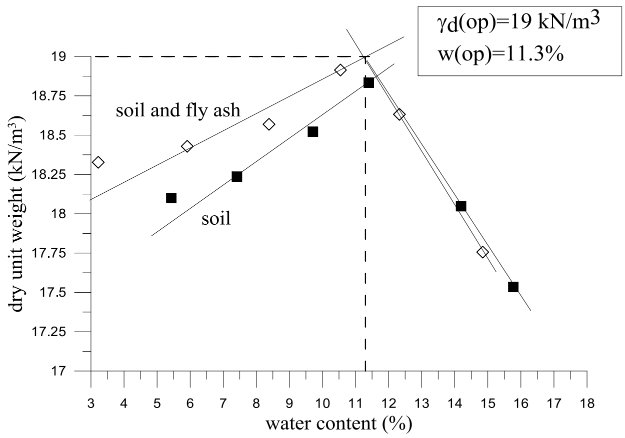

Figure 2. Modified Proctor curves of the soil and mixture of soil with 10% of fly ash

The properties of the mixtures are summarized in Table 1. The first mixture (C0) corresponds to soil and fly ash without activator compacted at the optimum condition with 11.3% of water content and 19 kN/m^3 of dry unit weight. The other 4 mixtures were molded considering an activator content of 11.3% for a sodium silicate over sodium hydroxide ratio of 0.5 (SS/SH=0.5). However, the concentration of the sodium hydroxide in the alkaline solution and the corresponding water content of these 4 mixtures varied.

Table 1. Mixtures composition

ID	Ash / solids (wt.)	NaOH concentration (molal)	Activ. content (%)	Water content (%)	Dry density (kN/m^3)
C0	0.10	-	-	11.3	19.00
C4	0.10	4	11.3	8.8	19.00
C6	0.10	6	11.3	8.4	19.00
C8	0.10	8	11.3	8.0	19.00
C10	0.10	10	11.3	7.7	19.00

In this new material water affects not only compaction but also the concentration of the alkaline solution. Increasing the water content reduces the concentration of the solution but increases the amount of water available for a better compaction. The evolution of stiffness and strength with NaOH concentration is analyzed in this paper.

2.3 Equipment and procedures

Seismic wave velocities measurements were performed on the specimens during curing at the following periods: 0, 3, 7, 14, 21 and 90 days. Compression and shear waves were measured by means of P and S wave ultrasonic transducers as described by Amaral et al. (2013). These transducers were linked to a signal generation and data acquisition Pundit lab unit from Proceq (http://www.proceq.com) connected to a laptop computer for display and data storage. To improve coupling between the transducer and the specimen, contact gel for ultrasound testing was used which highly improves the signal quality without damaging the specimen. In fact, one of the main advantages of these transducers is the easiness of application without holes in the specimen which could prevent the subsequent wave analysis or the unconfined compression tests performed at the end of curing periods. Several fixed frequencies were used ranging from 24 to 500 kHz. Depending on the specimen stiffness some led to clearer signals than others, but the propagation time was not sensitive to frequency, i.e, it was mostly constant with it.

At the end of the curing period (90 days) the specimens were tested in unconfined compression for strength evaluation. The tests were performed at 0.05 mm/min in an automatic loading machine of 100 kN of capacity together with a load cell of the same capacity and resolution of 0.006 kN. A lower velocity than the recommended in ASTM standard (ASTM, 1996) for this type of tests was considered in order to enable the execution of small unload-reload cycles at different compression stresses. The maximum stress of each cycle was 700 kPa, 1400 kPa, 2000 kPa and 2700 kPa which corresponds to 15%, 30%, 45% and 60% of 4700 kPa, being this value a conservative estimation of the unconfined compression strength of these mixtures. Local deformation transducers – LDTs (Goto et al., 1991) and Hall-Effect transducers (Viana da Fonseca et al., 2013) were used for accurate strain measurement during the test in order to provide reliable unload-reload stiffness moduli.

3 RESULTS

3.1 Unconfined compression strength tests

The stress-strain curves of the unconfined compression tests are presented in Figure 3. A significant difference is noticed between soil-ash specimen without alkali activation and the other specimens. In spite of the different water contents between soil ash specimens with and without the activator (around 8% and 11.3% respectively) the concentration of the alkaline activator proved to be the most important parameter. The unconfined compression strength increases with the concentration of the sodium hydroxide. The specimen with higher concentration (C10) also shows much higher overall stiffness, therefore a much smaller strain at peak, than the others. In fact, in this case, it was not possible to obtain unload-reload modulus in this particular specimen since the cycle strain (around 0.003%) was lower than the instrumentation resolution.

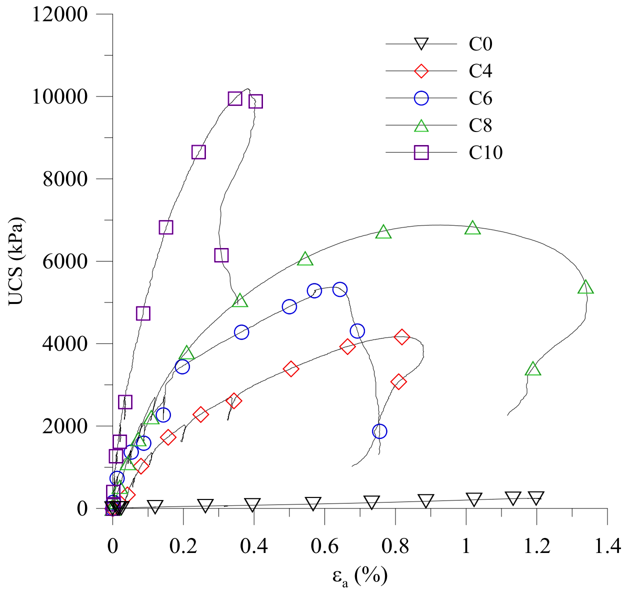

Figure 3. Stress-strain curves obtained in unconfined compression

The unload-reload moduli (E_{ur}) obtained from specimens C0, C4, C6 and C8 are presented in Table 2 together with the initial tangent moduli (E_{ti}) obtained for the same specimens using a hyperbolic curve fitting in the most initial values of the curve. E_{ti} values show a clear increase with the NaOH concentration in agreement with the unconfined compression strength trend indicating that both strength and stiffness are affected by the activator concentration. The unload-reload modulus evolution is explained by the combined effect of yielding and stress that evolves during compression loading. E_{ur} values tend to increase with mean effective stress state but at the same time stiffness tends to decrease with strain due to soil yielding and, bonding breakage in the cemented specimens (C4, C6, C8 and C10).

Table 2. Unload-reload modulus and initial tangent modulus

E MPa	E_{ti}	E_{ur} (1^{st}cycle)	E_{ur} (2^{nd}cycle)	E_{ur} (3^{rd}cycle)	E_{ur} (4^{th}cycle)
C0	2082	93	108	122	139
C4	4412	2644	2533	2490	2447
C6	6672	3908	4960	5070	5129
C8	8659	3274	3662	3615	3540
C10	-	-	-	-	-

Note: 1^{st}cycle ≈ 15% UCS; 2^{nd}cycle ≈ 30% UCS; 3^{rd}cycle ≈ 45% UCS; 4^{th}cycle ≈ 60% UCS

To remove the effect of stress state the unload-reload moduli were normalized by the mean effective stress of the cycle ($p'=\sigma'_1+2\sigma'_3)/3$) considered as one third of the average deviator stress of the cycle ($p'=q/3$). These results show continuous stiffness degradation from cycle to cycle in all bonded and unbonded specimens (Table 3). However, the stiffness degradation from the first to the second cycle is much higher in C0 than in the others where bonding is preventing a higher damage.

The secant modulus at 30% of the maximum strength ($E_{sec}^{30\%}$) was calculated as proposed in the European standard (CEN, 2003) and it presented in Figure 4 together with the initial tangent stiffness. The secant modulus values are significant lower than initial tangent stiffness moduli due to the different strain levels according to the material stiffness degradation pattern (Lo Presti, 1995, Gomes Correia et al, 2004, among others). Consequently, the ratio between these two moduli can give an indication of the degradation rate of bonding with strain level. $E_{sec}^{30\%}/E_{ti}$ ratios around 0.3 were observed for the three bonded specimens while a much lower value was obtained for C0 (0.01) indicating a significant degradation at 30% of strength.

Table 3. Normalized unload-reload modulus

	E_{ur}/p' (1^{st}cycle)	E_{ur}/p' (2^{nd}cycle)	E_{ur}/p' (3^{rd}cycle)	E_{ur}/p' (4^{th}cycle)
C0	55461	19981	12322	7016
C4	12630	6955	4375	3013
C6	17940	12103	8887	6310
C8	17207	8161	5901	4399
C10	-	-	-	-

Note: 1^{st}cycle ≈ 15% UCS; 2^{nd}cycle ≈ 30% UCS; 3^{rd}cycle ≈ 45% UCS; 4^{th}cycle ≈ 60% UCS

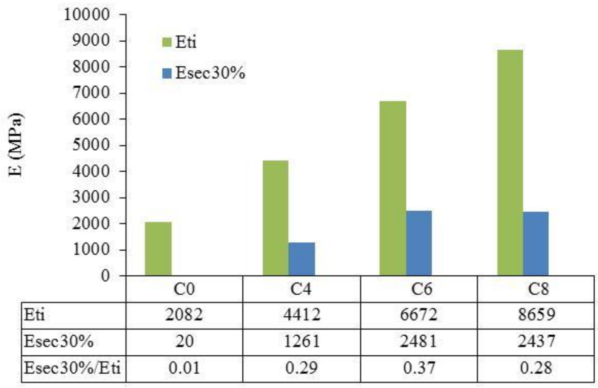

Figure 4. Comparison between initial tangent modulus (E_{ti}) and secant modulus at 30% of peak deviator stress ($E_{sec}^{30\%}$)

3.2 Seismic wave measurements

S and P wave measurements were performed on the bonded specimens at different curing times so that the stiffness evolution with time could be analyzed. Signals interpretation was performed by time domain analysis according to Viana da Fonseca et al. (2009). Since P waves are faster than S waves and were detected in the S wave signal, the first break detected in these signals corresponds to a P wave arrival. For that reason, S wave propagation time was detected later when a significant change in signal amplitude was noticed. Figure 5 illustrates S wave signals of the bonded specimens at 90 days of curing time where S and P wave propagation times are marked. It is clear that S wave propagation time is reducing (and so stiffness is increasing) when the activator concentration is increasing which is in agreement with the previous comments.

S and P wave velocities were calculated dividing the distance between transducers, i.e. the specimen's height, by the corresponding propagation time. The well-known expressions of the elasticity theory (equations 1, 2 and 3) enabled the calculation of the dynamic Young modulus (E_{din}).

$$G = \rho V_S^{\,2} \qquad (1)$$

$$\upsilon = \frac{\left(\frac{V_P}{V_S}\right)^2 - 2}{2\left(\frac{V_P}{V_S}\right)^2 - 2} \qquad (2)$$

$$E = 2G(1+\upsilon) \qquad (3)$$

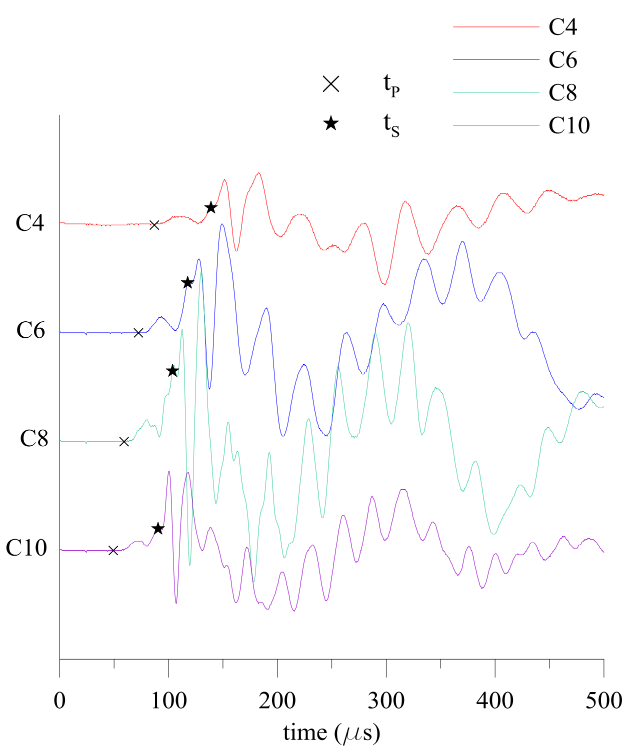

Figure 5. S wave signals at 90 days for specimens C4, C6, C8 and C10 with P and S wave propagation times respectively t_P and t_S

The evolution of E_{din} with curing time is illustrated in Figure 6 where significant increase with curing time is noticed in all specimens. This trend does not show evidence of stabilization even at 90 days, conversely to what is generally observed in soil-cement specimens (Rios, 2011), and more convergent to soil-lime mixtures (Viana da Fonseca and Castro Neves, 2011), these last with much smaller rate of increase.

The initial tangent stiffness (E_{ti}) calculated in the unconfined compression tests was compared with the dynamic Young modulus (E_{din}) at 90 days as expressed in Figure 7 for specimens C4, C6 and C8. E_{ti}/E_{din} ratios around 0.9 were observed for the three specimens indicating a small degree of degradation. Consequently it can be concluded that the hyperbolic curve fitting approach for the very initial points in the curves used to obtain the initial tangent modulus was able to derive a very high modulus in static conditions converging the maximum value in static conditions with the dynamic values, both assumed as purely elastic.

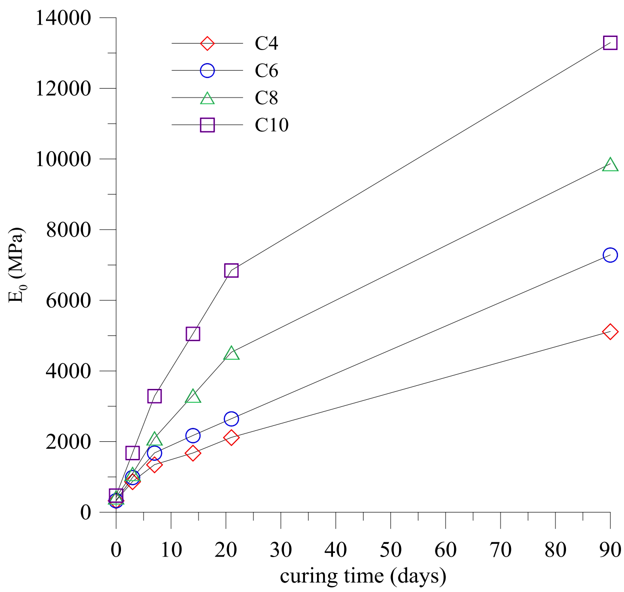

Figure 6. Evolution of the dynamic Young modulus with curing time

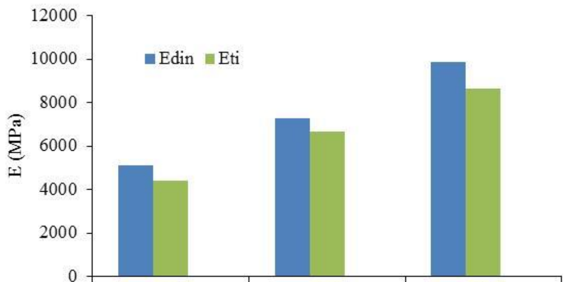

	C4	C6	C8
Edin	5117.48	7286.20	9866.45
Eti	4412.28	6672.45	8658.76
Eti/Edin	0.86	0.92	0.88

Figure 7. Comparison between dynamic Young modulus (E_{din}) and initial tangent modulus (E_{ti}) at 90 days of curing time

4 CONCLUSIONS

Alkaline activation of fly ash for soil improvement was studied to evaluate its potential as a stabilization technique without Portland cement or lime, both involving high CO_2 emissions. For that purpose, specimens of Porto silty sand and fly ash mixed with an alkaline solution in different concentrations were prepared and tested in unconfined compression (UCS) at 90 days for strength analysis. Stiffness properties were also accessed performing UCS tests with local strain measurements so that stiffness modulus could be derived as well as by means of seismic wave measurements. Being a non-destructive technique it allowed the evaluation of the dynamic stiffness evolution with curing time without inducing any damage to the specimen.

The unconfined compression strength and initial tangent stiffness from UCS tests showed a significant increase with the alkaline solution concentration up to 8 times for the highest concentration. Seismic wave measurements showed a continuous evolution of E_{din} with curing time in all bonded specimens. This trend did not show evidence of stabilization since the stiffness at 90 days doubled the value at 28 days, conversely to what is generally observed in soil-cement mixtures and converging with long term evolution of soil-lime mixtures.

These results illustrate the potential of this technique for soil stabilization since soil stiffness and strength are considerably improved without cement or lime addition and consequently, without CO_2 production, while including a waste material like fly ash.

ACKNOWLEDGEMENTS

The authors would like to acknowledge Pegop – Energia Eléctrica, SA which runs the thermoelectric power plant of Pego, for the supply of fly ash.

REFERENCES

Alonso S. and Palomo A. (2001). Alkaline activation of metakaolin and calcium hydroxide mixtures: influence of temperature, activator concentration and solids ratio, *Materials Letters*, Vol. 47, p. 55-62.

Amaral, M. F., Viana da Fonseca, A., and Rios, S. (2013). Numerical Methodology to Minimize Resolution and Sensitivity Effects in P-Wave Measurements, *Geotechnical Testing Journal*, Vol. 36, No. 2, pp. 1–10, doi:10.1520/GTJ20120111. ISSN 0149-6115.

ASTM (1996). D 1633-96. Standard test method for compressive strength of molded soil-cement cylinders.

ASTM. (1998). Standard practice for classification of soils for engineering purposes (Unified Soil Classification System). D2487-98, West Conshohocken, PA.

CEN (2003). EN 13286-43 - Unbound and hydraulically bound mixtures - Part 43: Test method for the determination of the modulus of elasticity of hydraulically bound mixtures, Comité Européen de Normalisation, Brussels

Cristelo N., Glendinning S., and Teixeira Pinto A. (2011). Deep soft soil improvement by alkaline activation, *Proceedings of the ICE - Ground Improvement*, Vol. 164, No.2, pp. 73-82.

Cristelo, N., Glendinning, S., Fernandes, L. and Teixeira Pinto, A. (2013). Effects of Alkaline-Activated Fly Ash and Portland Cement on Soft Soil Stabilisation. *Acta Geotechnica*, Vol. 8, p. 395-405.

Duncan, J.M. and Chang, C.-Y. (1970). Nonlinear Analysis of Stress and Strain in Soil. *ASCE J. of the Soil Mech. and Found. Div.*, Vol. 96, p. 1629-1653.

Gomes Correia, A., Viana da Fonseca, A. and Gambin, M. (2004). Routine and advanced analysis of mechanical in-situ tests. Results on saprolitic soils from granites more or less mixed in Portugal. *Proc. Geotechnical and Geophysical Site Characterization*, Keynote Lecture, Viana da Fonseca, A. and Mayne, P.W.(eds.) Millpress, Rotterdam, Vol. 1, p. 75-96.

Goto, S, Tatsuoka, F, Shibuya, S, Kim, Y-S, Sato, T. (1991). A simple gauge for local small strain measurements in the laboratory. *Soils and Foundations*, Vol. 31, No.1, p. 169-180.

Ingold, T.S. and Miller, K.S. (1983). Drained Axisymmetric Loading of Reinforced Clay, *Journal of Geotechnical Engineering*, ASCE, Vol. 109, p. 883-898.

Lo Presti, D. (1995). General Report: Measurements of Shear Deformation of Geomaterials in the Laboratory. *Pre-failure Deformation of Geomaterials*, Shibuya, Mitachi & Miura (eds), Balkema, Rotterdam, Vol. 2, p. 1067-1088

Rios, S. (2011). A general framework for the geomechanical characterisation of artificially cemented soil. PhD thesis, Faculty of Engineering, University of Porto.

Viana da Fonseca, A., Ferreira, C., and Fahey, M. (2009). A Framework Interpreting Bender Element Tests, Combining Time-Domain and Frequency-Domain Methods. *Geotechnical Testing Journal*, Vol. 32, No.2, p.

Viana da Fonseca, A. and Castro Neves, N. (2011) Evolução no tempo do comportamento mecânico de solos melhorados com cal aérea". *Revista Geotecnia*, Vol. 122, p. 31-47

Viana da Fonseca, A., Rios, S. and Amaral, M. F. (2013). Structural anisotropy by static compaction, *Engineering Geology*, Vol. 154, p. 89-97, http://dx.doi.org/10.1016/j.enggeo.2012.11.012.

Worrell, E., Price, L., Martin, N., Hendriks, C. and Meida, L.O. (2001). Carbon Dioxide Emissions from the Global Cement Industry, *Annual Review of Energy and the Environment*, Vol. 26, No. 1, p. 303-29.